

Effects of Ce, Y and Gd additions on as-cast microstructure and mechanical properties of Mg–3Sn–2Sr magnesium alloy

Ming-bo YANG^{1,2,3}, Meng-dan HOU², Jia ZHANG², Fu-sheng PAN³

1. Key Laboratory of Manufacture and Test Techniques for Automobile Parts, Ministry of Education, Chongqing University of Technology, Chongqing 400054, China;

2. Materials Science and Engineering College, Chongqing University of Technology, Chongqing 400054, China;

3. National Engineering Research Center for Magnesium Alloys, Chongqing University, Chongqing 400030, China

Received 22 July 2013; accepted 19 October 2013

Abstract: The effects of Ce, Y and Gd additions on the as-cast microstructure and mechanical properties of Mg–3Sn–2Sr alloy were investigated and compared by scanning electron microscopy, X-ray diffraction, differential scanning calorimetry analysis, tensile and creep tests. The results indicate that the Mg–3Sn–2Sr ternary alloy is mainly composed of α -Mg, primary and eutectic SrMgSn, and Mg₂Sn phases. After the additions of 1.0% Ce, 1.0% Y and 1.0% Gd to the Mg–3Sn–2Sr alloy, the Mg₁₂Ce, YMgSn, GdMgSn and/or Mg₁₇Sr₂ phases are formed, respectively. At the same time, the formation of the primary SrMgSn phase is suppressed and the coarse needle-like primary SrMgSn phase is modified and refined. In addition, the additions of 1.0% Ce, 1.0% Y and 1.0% Gd to the Mg–3Sn–2Sr alloy can simultaneously improve the tensile and creep properties of the alloy. Among the Ce-, Y- and Gd-containing alloys, the tensile properties of the Ce-containing alloy are relatively higher than those of the Y- and Gd-containing alloys.

Key words: Mg–Sn–Sr alloys; Ce; Y; Gd; SrMgSn phase

1 Introduction

It is well known that the improvement in the elevated temperature properties for magnesium alloys has become a critical issue for possible application in hot components [1]. Recent investigations have indicated that Mg–Sn–Sr alloys are likely to have great potential in the development of creep-resistant magnesium alloys due to the following reasons [2–10]: 1) Sn not only behaves as a grain refiner but also can improve the corrosion resistance and form a stable Mg₂Sn compound with Mg [3–5]; 2) Sr not only behaves as a grain refiner but also can form some stable Mg₁₇Sr₂, Mg₂₃Sr₆, Mg₃₈Sr₉ and Mg₂Sr phases with Mg due to the low solid solubility of Sr in Mg (0.11%, mass fraction) [6–8]; 3) Sr and Sn together with Mg may form the stable intermetallic compound SrMgSn which has higher thermal stability than the Mg₂Sn phase [9,10]. However, up to now, the investigations about the microstructures

and mechanical properties of Mg–Sn–Sr ternary alloys are very limited. In addition, the potential for further improvement in strength and creep-resistant performance via further alloying/microalloying additions for Mg–Sn–Sr ternary alloys is also very scarce. It is well known that rare earth (RE) elements such as Ce, Y and Gd in Mg–Sn based alloys can show favorable effects on the mechanical properties. For example, YANG et al [3] found that Ce, Y and/or Gd additions to the Mg–3Sn–1Mn (mass fraction, %) alloy could effectively improve the tensile and creep properties of the alloy. At the same time, GRONY et al [11] reported that the Mg–Sn–Zn–Y quaternary alloys exhibited good comprehensive mechanical properties in wider temperature range due to the presence of several stable intermetallic compounds such as YMgSn. In addition, SHI et al [12] found that Gd addition to the Mg–5Sn–1Ca alloy could form the GdMgSn phase with high thermal stability and thus results in the enhanced elevated temperature properties. Therefore, it is expected that Ce, Y and Gd additions

Foundation item: Project (CSTC2013jcyjC60001) supported by the Chongqing Science and Technology Commission of China; Project (KJ120834) supported by the Chongqing Education Commission of China; Project (CQUT1205) supported by the Open Funds from Key Laboratory of Manufacture and Test Techniques for Automobile Parts, Ministry of Education, Chongqing University of Technology, China

Corresponding author: Ming-bo YANG; Tel: +86-23-62563176; E-mail: yangmingbo@cqut.edu.cn

DOI: 10.1016/S1003-6326(14)63376-8

possibly play a beneficial role in the mechanical properties of Mg–Sn–Sr ternary alloys. Due to the above mentioned reasons, the present work investigates and compares the effects of Ce, Y and Gd additions on the as-cast microstructure and mechanical properties of Mg–3Sn–2Sr ternary alloy.

2 Experimental

The Ce-, Y- and Gd-containing Mg–3Sn–2Sr experimental alloys were prepared from commercially pure Mg and Sn (>99.9%, mass fraction), and Sr, Ce, Y and Gd were respectively added in the form of Mg–10%Sr, Mg–29%Ce, Mg–17%Y and Mg–24.5%Gd master alloys. In this work, the single content of Ce, Y and Gd additions, 1.0% (mass fraction), was preliminarily selected due to the following considerations: 1) in the previous investigations about the effects of Ce, Y and Gd additions on the as-cast microstructure and mechanical properties of the Mg–3Sn–2Ca ternary alloy [13–15], the relatively optimal amount of Ce, Y and Gd addition is about 1.0%, respectively, and 2) although the chemical compositions of the Mg–3Sn–2Ca and Mg–3Sn–2Sr ternary alloys are different, the two alloys belong to Mg–Sn based alloys, and the chemical and metallurgical properties of Sr and Ca are basically similar [6]. Therefore, a similar content of Ce, Y and Gd addition, 1.0%, is possibly suitable for the Mg–3Sn–2Sr ternary alloy. The experimental alloys were melted at 730–750 °C in a crucible resistance furnace and protected by 2% (mass fraction) RJ-2 flux additions. After Ce, Y or Gd were added to the melt at 740 °C, the melt was held at 740 °C for 10 min and then poured into a low-carbon steel mould coated and preheated to 200 °C in order to obtain a casting as shown in Fig. 1. The specimens whose sizes have been reported in Ref. [16] were fabricated from the casting for tensile and creep tests. For comparison, the Mg–3Sn–2Sr alloy without the additions of Ce, Y and Gd was also cast and machined into the same dimensions and tested under the same conditions as the above samples. Table 1 lists the actual chemical compositions of the experimental alloys,



Fig. 1 Casting for mechanical properties tests

Table 1 Actual compositions of experimental alloys (mass fraction, %)

Alloy No.	Nominal alloy	Sn	Sr	Ce	Y	Gd	Mg
1 [#]	Mg–3Sn–2Sr	2.90	1.86	–	–	–	Bal.
2 [#]	Mg–3Sn–2Sr+1.0Ce	2.92	1.88	0.93	–	–	Bal.
3 [#]	Mg–3Sn–2Sr+1.0Y	2.91	1.85	–	0.88	–	Bal.
4 [#]	Mg–3Sn–2Sr+1.0Gd	2.92	1.89	–	–	0.89	Bal.

which were inspected by inductively coupled plasma spectroscopy.

In order to analyze the solidification behavior of the experimental alloys, the differential scanning calorimetry (DSC) was carried out by using a NETZSCH STA 449C system equipped with platinum–rhodium crucibles. A 30 mg (± 0.1 mg) sample for each examined specimens was heated in a flowing argon atmosphere from 30 to 700 °C for 5 min before being cooled down to 100 °C. The cooling curves were recorded at a controlling speed of 15 °C/min.

The as-cast samples were etched with an 8% nitric acid solution, and then examined by using an Olympus optical microscope and JEOL/JSM-6460LV scanning electron microscope (SEM). The phases in the experimental alloys were analyzed by D/Max–1200X type X-ray diffraction (XRD). The tensile properties at room temperature and 150 °C for the as-cast experimental alloys were determined from a stress–strain curve. The ultimate tensile strength (UTS), 0.2% yield strength (YS) and elongation to failure (Elong.) were obtained based on the average of three tests under the strain rate of 0.1 s^{−1}. The constant-load tensile creep tests of the as-cast experimental alloys were carried out at a constant temperature between 150 °C and 200 °C and a constant applied stress between 50 and 80 MPa. The tests were performed until the specimen broke or the minimum creep rate reached. The total creep strain and minimum creep rates of the as-cast experimental alloys were respectively measured from each elongation versus time curve and averaged over three tests.

3 Results and discussion

3.1 As-cast microstructures

Figure 2 shows the XRD results of the as-cast alloys. As shown in Fig. 2, the Mg–3Sn–2Sr ternary alloy is mainly composed of α -Mg, SrMgSn and Mg₂Sn phases. The Mg₁₇Sr₂ phase which commonly forms in Mg–Sr based alloys [6], is not observed in the XRD results of the Mg–3Sn–2Sr ternary alloy. Furthermore, it is found from Fig. 2 that the additions of 1.0% Ce, 1.0% Y or 1.0% Gd to the Mg–3Sn–2Sr alloy lead to the formation of the extra phases of Mg₁₂Ce, YMgSn and GdMgSn, respectively, therinto the YMgSn and

GdMgSn phases have been reported in the Y- and Gd-containing Mg–Sn based alloys [3] and described in detail in Ref. [17].

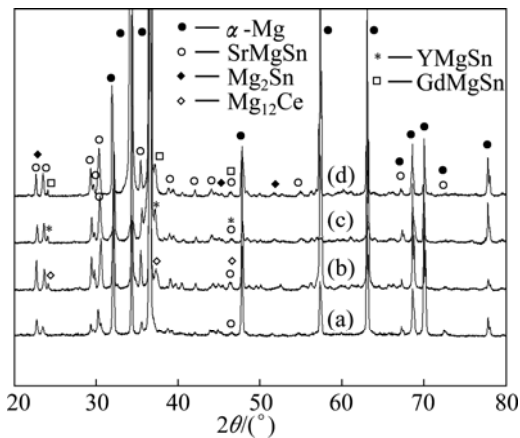


Fig. 2 XRD patterns of as-cast alloys: (a) 1[#] alloy; (b) 2[#] alloy; (c) 3[#] alloy; (d) 4[#] alloy

Figures 3 and 4 show the low and high magnification SEM images of the as-cast alloys, respectively. Combining the XRD and EDS results (Table 2), the main intermetallic compounds in Fig. 4 are identified as Mg₂Sn, SrMgSn, Mg₁₂Ce, YMgSn, GdMgSn and Mg₁₇Sr₂ phases. In Figs. 3 and 4, two types of the SrMgSn phases with different morphologies are observed. One is the primary SrMgSn phase with a typical particle-, needle- and short rod-like morphologies. The other is the eutectic SrMgSn phase with a typical feather-like morphology. Figure 5 shows the DSC cooling curves of the as-cast alloys. It is found from Fig. 5 that the DSC cooling curves of the experimental

alloys are similar, with two main peaks of *A* and *B* in the cooling curves, indicating that the additions of 1.0% Ce, 1.0% Y or 1.0% Gd to the Mg–3Sn–2Sr ternary alloy do not influence the types of the phase transformations of the alloy. Similar to the previous analysis [2], it is preliminarily inferred from Fig. 5 that during the solidification of the Mg–3Sn–2Sr ternary alloy, the primary SrMgSn phase first nucleates and grows when passing through *L*+SrMgSn region in the hypereutectic composition range [10] (at present, the temperature of phase transformation for the formation of primary SrMgSn phase is unclear), and then the α -Mg phase begins to nucleate and grow at 620–630 °C corresponding to the peak *A*. Then, along with the temperature decreasing the eutectic SrMgSn phase begins to precipitate at about 570 °C corresponding to the peak *B* [9]. In this case, if Sn is not used up during the formation of the primary and eutectic SrMgSn phases, the binary eutectic reaction ($L \rightarrow \alpha\text{-Mg} + \text{Mg}_2\text{Sn}$) would take place at about 530 °C [12] and then Mg₂Sn phase with small amount would be formed. Accordingly, the final microstructure of the Mg–3Sn–2Sr ternary alloy mainly consists of α -Mg, primary and eutectic SrMgSn, and Mg₂Sn phases. As for the reason why there is no obvious peak corresponding to the Mg₂Sn phase for the Mg–3Sn–2Sr ternary alloy, it is possibly related to the small amount of the phase in the alloy. Furthermore, simple visual comparison of these images in Figs. 3 and 4 shows that the volume fraction of the primary SrMgSn phases in the Ce-, Y- and Gd-containing alloys seems to be relatively lower than those in the ternary alloy, indicating that the additions of 1.0% Ce, 1.0%Y or 1.0% Gd to the Mg–3Sn–2Sr alloy possibly suppress the

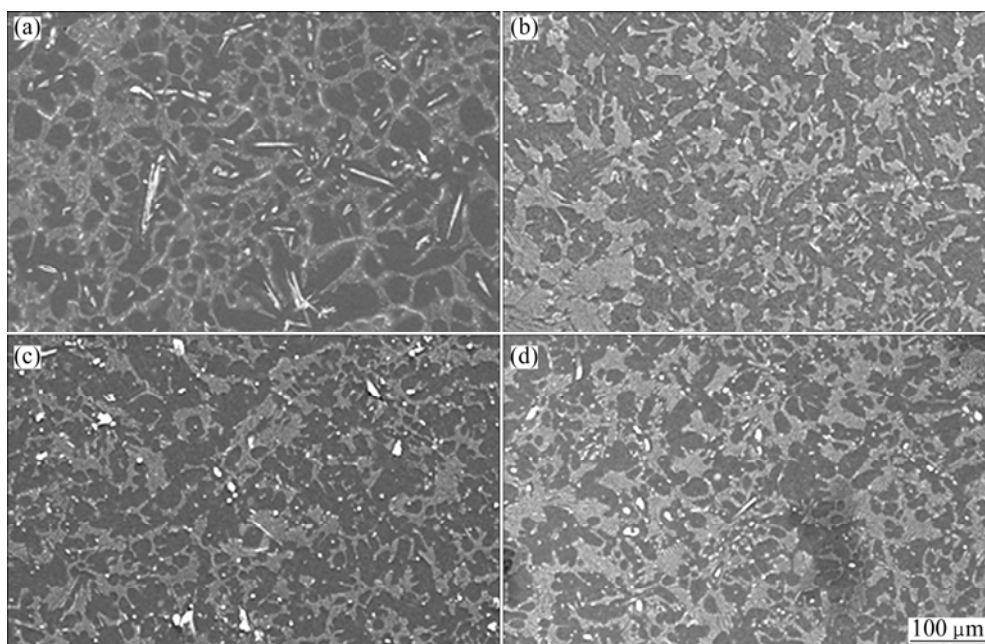


Fig. 3 Low magnification SEM images of as-cast alloys: (a) 1[#] alloy; (b) 2[#] alloy; (c) 3[#] alloy; (d) 4[#] alloy

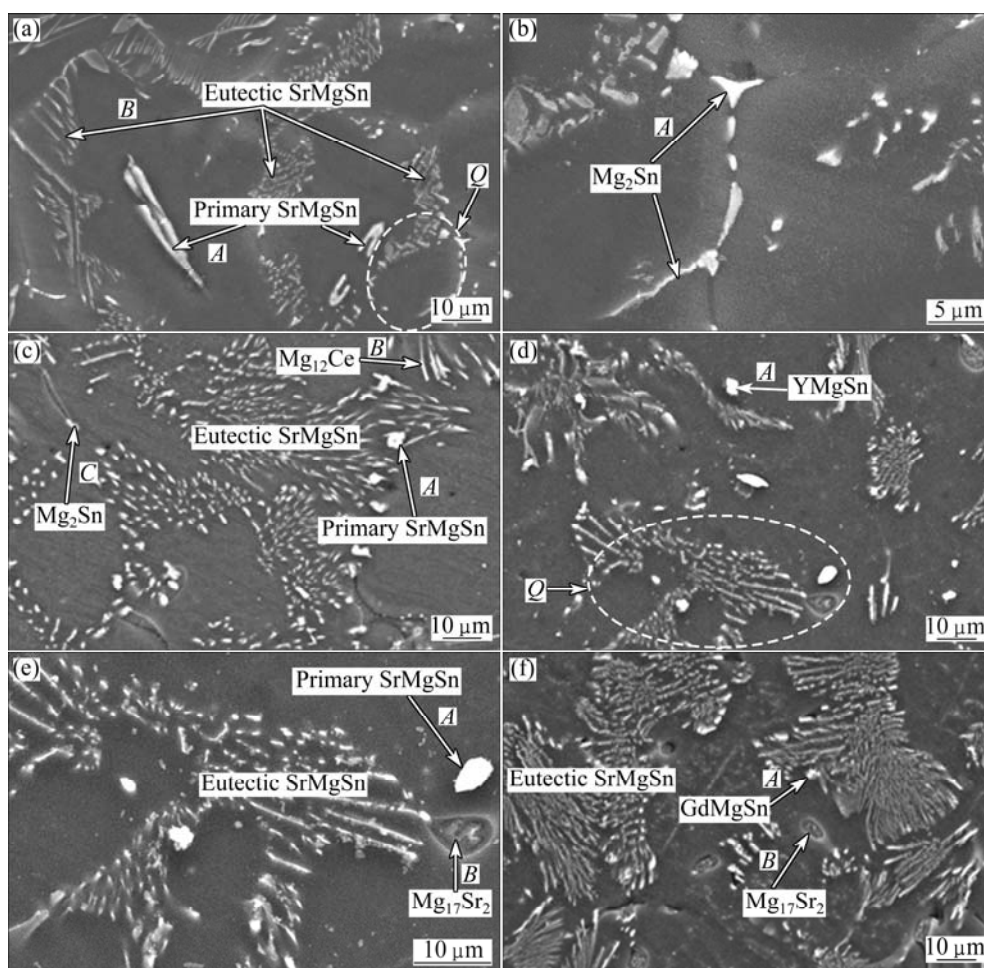


Fig. 4 High magnification SEM images of as-cast alloys: (a) 1[#] alloy; (b) Local magnification of area *Q* in (a); (c) 2[#] alloy; (d) 3[#] alloy; (e) Local magnification of area *Q* in (d); (f) 4[#] alloy

Table 2 EDS results of as-cast alloys

Position	Composition (mole fraction)/%						Possible compound
	Mg	Sn	Sr	Ce	Y	Gd	
Fig. 4(a)-A	60.45	25.32	14.23	–	–	–	SrMgSn
Fig. 4(a)-B	62.18	24.76	13.06	–	–	–	SrMgSn
Fig. 4(b)-A	70.24	29.68	0.08	–	–	–	Mg ₂ Sn
Fig. 4(c)-A	58.36	26.22	14.18	1.24	–	–	SrMgSn
Fig. 4(c)-B	67.97	5.56	–	26.47	–	–	Mg ₁₂ Ce
Fig. 4(c)-C	71.51	28.49	–	–	–	–	Mg ₂ Sn
Fig. 4(d)-A	38.54	30.23	–	–	31.23	–	YMgSn
Fig. 4(e)-A	58.21	25.44	15.03	–	1.32	–	SrMgSn
Fig. 4(e)-B	70.05	0.04	29.91	–	–	–	Mg ₁₇ Sr ₂
Fig. 4(f)-A	46.87	25.32	–	–	–	27.81	GdMgSn
Fig. 4(f)-B	67.98	0.82	30.17	–	–	1.03	Mg ₁₇ Sr ₂

formation of the primary SrMgSn phase. In addition, it is found from Figs. 3 and 4 that the primary SrMgSn phases in the Mg–3Sn–2Sr ternary alloy mainly exhibit the fine particle-, coarse needle- and short rod-like

morphologies. However, in the Ce-, Y- and Gd-containing alloys only the primary SrMgSn phases with the fine particle- and short rod-like morphologies are observed, indicating that the additions of 1.0% Ce, 1.0% Y or 1.0% Gd to the Mg–3Sn–2Sr alloy can modify and refine the coarse needle-like primary SrMgSn phase. This is possibly related to the following two aspects: 1) the volume fraction of the primary SrMgSn phases in the Ce-, Y- and Gd-containing alloys decreases; 2) the formation of the Mg₁₂Ce, YMgSn and GdMgSn compounds in the Ce-, Y- and Gd-containing alloys possibly restrains the growth of the primary SrMgSn phase during the solidification due to their high melting point and heat resistance [3, 13–15]. In addition, the modification and refinement of the primary SrMgSn phase in the Ce-containing alloy are possibly related to the Ce enrichment which hinders the Sn atom diffusion and induces the constitution undercooling at the solidification interface front due to the low solid solubility of Ce in Mg (1.6%).

In addition, in Fig. 4(c) the Mg₁₂Ce phases with the

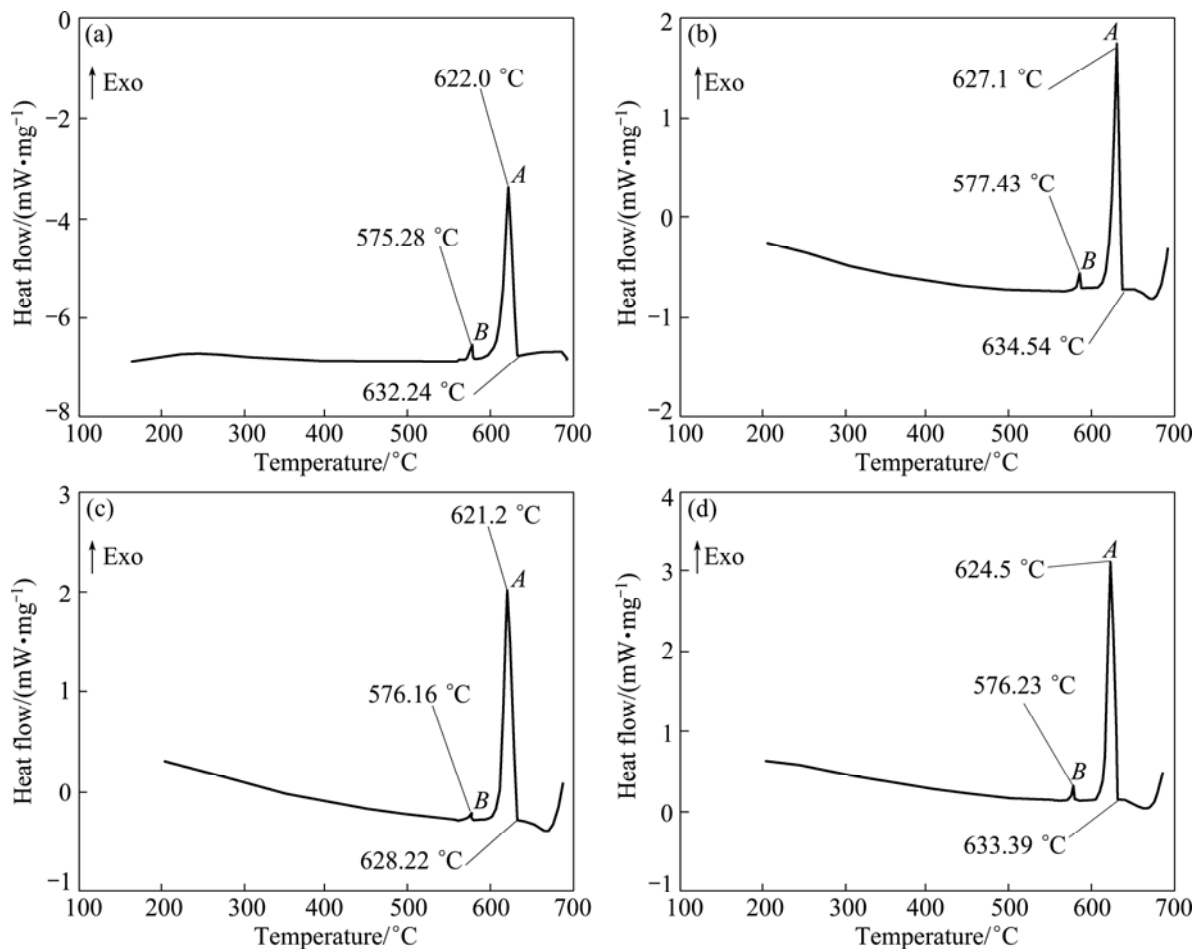


Fig. 5 DSC cooling curves of as-cast alloys: (a) 1[#] alloy; (b) 2[#] alloy; (c) 3[#] alloy; (d) 4[#] alloy

short rod-like morphology are observed in the Ce-containing alloy. At the same time, in Figs. 4(d)–(f) the particle-like shaped YMgSn and GdMgSn phases with small amount are also detected in the Y- and Gd-containing alloys, respectively. Furthermore, it is found from Figs. 4(d)–(f) that the Y- and Gd-containing alloys contain small amounts of Mg₁₇Sr₂ phase with the particle-like shapes although the phase is not detected in the XRD results of the two alloys. It is well known that the solid solubilities of Y, Gd and Sn elements in α -Mg matrix are relatively high (Y: 12.6%; Gd: 23.5%; Sn: 14.85%, mass fraction), and both Y and Gd atoms have relatively larger atomic radius than Sn atom (Y: 0.182 nm; Gd: 0.178 nm; Sn: 0.141 nm). Therefore, after Y or Gd additions to the Mg–3Sn–2Sr alloy, Y and Gd elements possibly hinder Sn atom diffusion from the α -Mg matrix to the grain boundaries. In addition, Y and Gd additions to the Mg–3Sn–2Sr alloy result in the formation of the YMgSn and GdMgSn phases, respectively. The two factors possibly cause a decrease in the amount of Sn distributed at grain boundaries, which is one of the possible reasons for the formation of the Mg₁₇Sr₂ phases in the Y- and Gd-containing alloys.

3.2 Tensile properties

Figure 6 shows the typical tensile stress–strain curves of the as-cast alloys tested at room temperature and 150 °C. The tensile properties at room temperature and 150 °C, including ultimate tensile strength (UTS), 0.2% yield strength (YS) and elongation (Elong.), are listed in Table 3. It is observed that the tensile properties at room temperature and 150 °C for the Ce-, Y- and Gd-containing alloys are higher than those for the ternary alloy, indicating that the additions of 1.0% Ce, 1.0% Y or 1.0% Gd to the Mg–3Sn–2Sr ternary alloy can improve the tensile properties of the alloy. It is well known that the fine and uniform phases distributed along the grain boundaries are easier to act as effective straddle to the dislocation motion, thus improving the properties of engineering alloys [18]. Apparently, the relatively coarse needle-like shaped SrMgSn phases in the ternary alloy would give a detrimental effect on the mechanical properties since the cracks can easily nucleate along the interface between the primary SrMgSn particle and α -Mg matrix [2,9]. However, after the additions of 1.0% Ce, 1.0% Y or 1.0% Gd to the Mg–3Sn–2Sr ternary alloy, the coarse needle-like shaped SrMgSn

phases are effectively modified and refined (Figs. 3 and 4), then the extending tendency of microcracks will decrease. Accordingly, the tensile properties of the Ce-, Y- and Gd-containing alloys are improved. Of course, the $Mg_{12}Ce$, $YMgSn$ and $GdMgSn$ phases in the Ce-, Y- and Gd-containing alloys possibly play an important role in the improvement of tensile properties. Furthermore, it is found from Table 3 that among the Ce-, Y- and Gd-containing alloys the tensile properties at room

temperature and 150 °C for the Ce-containing alloy are relatively higher than those for the Y- and Gd-containing alloys. This is possibly related to the formation of the $YMgSn$ and $GdMgSn$ phases in the Y- and Gd-containing alloys, which possibly cause a decrease in the amount of Sn dissolved in the α -Mg matrix and then leads to the decrease of the strength of the α -Mg matrix. However, this needs to be further confirmed. Figure 7 shows the SEM images of the tensile fractographs for the

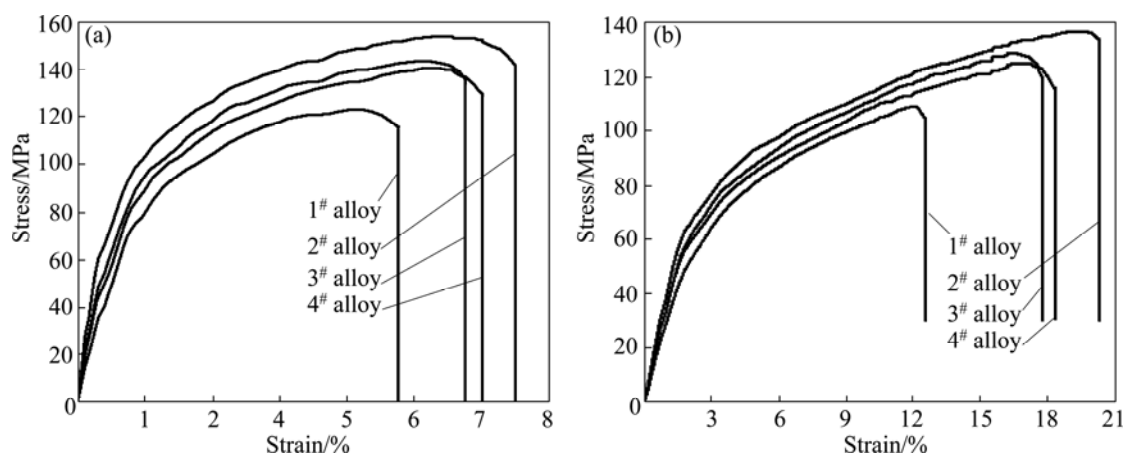


Fig. 6 Typical tensile stress–strain curves of as-cast alloys: (a) Room temperature; (b) 150 °C

Table 3 Tensile properties of as-cast alloys tested at room temperature and 150 °C

Alloy No.	Room temperature			150 °C		
	UTS/MPa	YS/MPa	Elong/%	UTS/MPa	YS/MPa	Elong/%
1 [#]	124±2.2	94±2.4	2.9± 0.16	111±2.1	82±3.8	12.5±1.2
2 [#]	153±1.8	117±1.7	4.6± 0.18	137±3.6	104±3.2	20.0± 1.1
3 [#]	144±3.1	103±2.6	4.2± 0.23	130±1.9	93±2.6	16.9± 2.4
4 [#]	141±2.4	108±1.2	4.3±0.19	125±3.4	96±1.5	17.3± 1.6

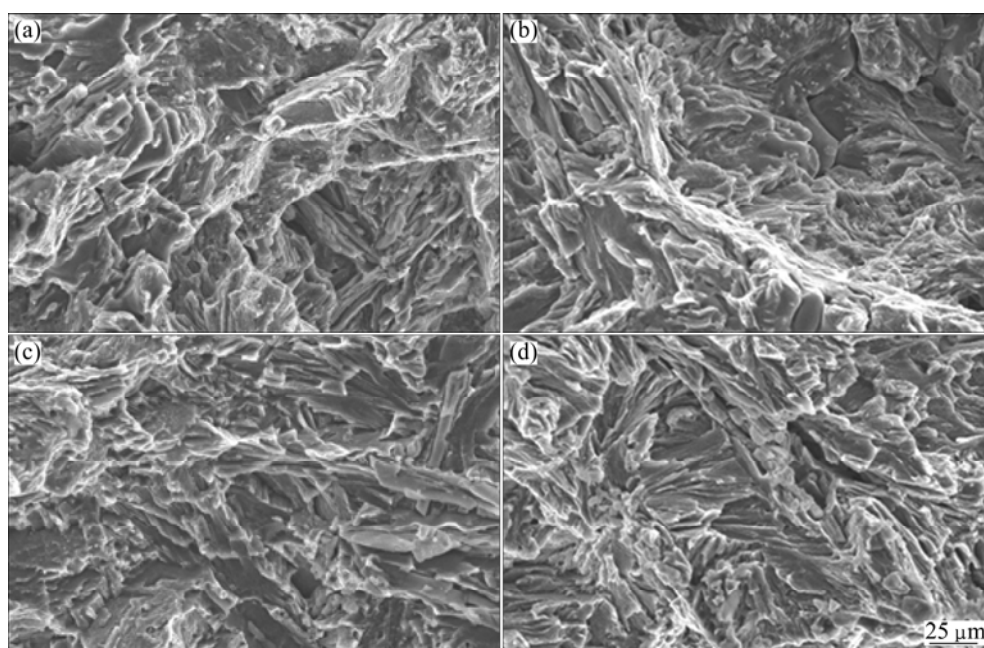


Fig. 7 SEM fractographs of as-cast alloys tested at room temperature: (a) 1[#] alloy; (b) 2[#] alloy; (c) 3[#] alloy; (d) 4[#] alloy

as-cast alloys failed in the tensile tests at room temperature. As shown in Fig. 7, a number of cleavage planes and steps are present, and some river patterns can also be observed on the tensile fracture surfaces of the experimental alloys, indicating that all the tensile fracture surfaces have mixed characteristics of cleavage and quasi-cleavage fractures. Obviously, the additions of 1.0% Ce, 1.0% Y or 1.0% Gd to the Mg–3Sn–2Sr ternary alloy do not significantly change the fracture mode of the alloy.

3.3 Creep properties

Figure 8 shows the typical creep strain curves of the as-cast alloys tested at 150 °C and 70 MPa for 100 h. The creep properties, including total creep strain and minimum creep rate, are listed in Table 4. As listed in Table 4, the Mg–3Sn–2Sr ternary alloy exhibits relatively high creep properties. It is well known that the steady-state creep rate ($\dot{\epsilon}$) can be explained by the power-law relationship reported in Ref. [19]. At the same time, both the stress exponent (n) and activation energy (Q) might be determined from the creep data collected at various temperatures and stresses, and might be used together to identify the dominant creep mechanism of a material [19]. In order to determine the stress exponent (n) and activation energy (Q) of the Mg–3Sn–2Sr ternary alloy, the slope of a plot of $\lg \dot{\epsilon}$ vs $\lg \sigma$ and $\ln \dot{\epsilon}$ as a function of $1/T$ were evaluated. Figure 9 shows the slopes of the stress exponent and activation energy of the Mg–3Sn–2Sr ternary alloy. As shown in Fig. 9(a), at low stress the stress exponent of the Mg–3Sn–2Sr ternary alloy is 5.6 but 6.8 at high stress. The estimated activation energy at 70 MPa for the Mg–3Sn–2Sr ternary alloy is 110.4 kJ/mol (Fig. 9(b)). These values indicate that under the present test conditions the creep deformation of the Mg–3Sn–2Sr ternary alloy mainly occurs through the dislocation climb due to the following reasons [10,20]: 1) the stress exponent $n=4-6$ is thought

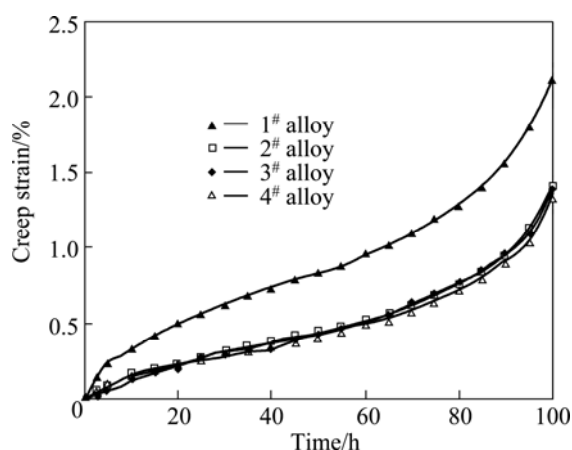


Fig. 8 Typical creep strain curves of as-cast alloys tested at 150 °C and 70 MPa for 100 h

Table 4 Creep properties of as-cast alloys tested at 150 °C and 70 MPa for 100 h

Alloy No.	Total creep strain/%	Minimum creep rate, $\dot{\epsilon}_{\min}/10^{-8} \text{ s}^{-1}$
1#	2.12±0.05	5.88±0.31
2#	1.40±0.07	3.89±0.34
3#	1.37±0.04	3.80±0.17
4#	1.39±0.11	3.86±0.22

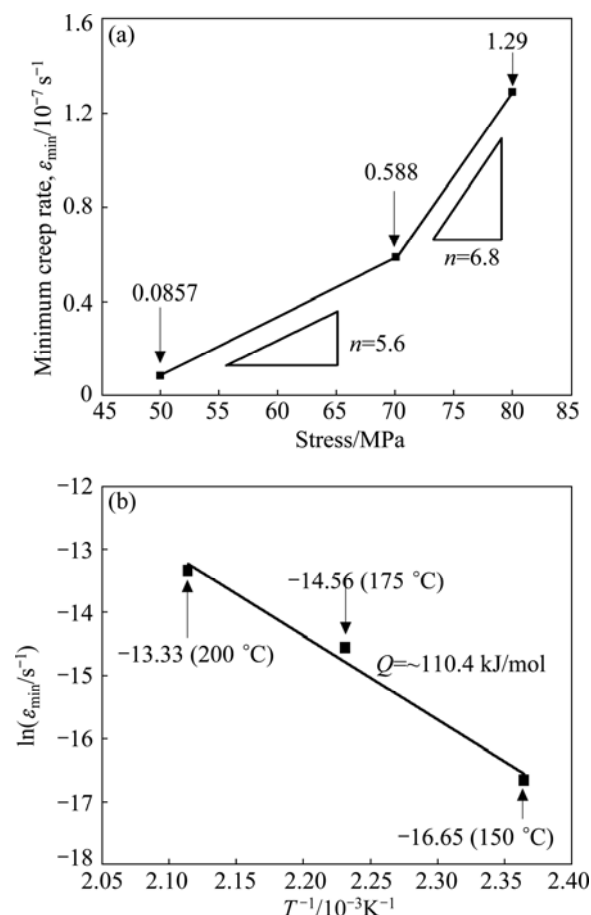


Fig. 9 Applied stress and temperature dependence of minimum creep rate for as-cast Mg–3Sn–2Sr ternary alloy: (a) Applied stresses with 50 MPa, 70 MPa and 80 MPa at 150 °C; (b) Applied temperatures at 150 °C, 175 °C and 200 °C with 70 MPa

to be mainly related to the dislocation climb controlled creep; 2) the activation energy of the Mg–3Sn–2Sr ternary alloy is relatively higher than that of the grain boundary diffusion (92 kJ/mol) and cross slip (100 kJ/mol) for magnesium alloys deformed by grain boundary diffusion, but is relatively lower than that of the lattice self-diffusion (135 kJ/mol) for magnesium alloys deformed by dislocation climb. Figure 10 shows the SEM images of the as-cast alloys after creep test at 150 °C and 70 MPa for 60 h. As shown in Fig. 10(a), the SrMgSn phases in the Mg–3Sn–2Sr ternary alloy seem

to have little change, indicating that the thermal stability of the SrMgSn phase is high. In general, an increase in the volume fraction of thermal stability phases for magnesium alloys results in an increase in creep properties. Therefore, the thermally stable SrMgSn phases in the Mg–3Sn–2Sr ternary alloy pin the grain boundaries and hinder both grain boundary migration and sliding during high temperature deformation. Accordingly, the Mg–3Sn–2Sr ternary alloy exhibits high creep properties. Furthermore, it is observed from Table 4 that the creep properties of the Ce-, Y- and

Gd-containing alloys are similar, and they are relatively higher than those of the ternary alloy, indicating that the additions of 1.0% Ce, 1.0% Y and 1.0% Gd to the Mg–3Sn–2Sr ternary alloy can improve the creep properties of the alloy, respectively. Based on the above analysis, the thermally stable SrMgSn phases in the Ce-, Y- and Gd-containing alloys can also make a contribution to the high creep properties of the three alloys. Furthermore, from the optical images of the longitudinal sections for the as-cast alloys obtained after creep rupture at 150 °C and 70 MPa (Fig. 11), it is

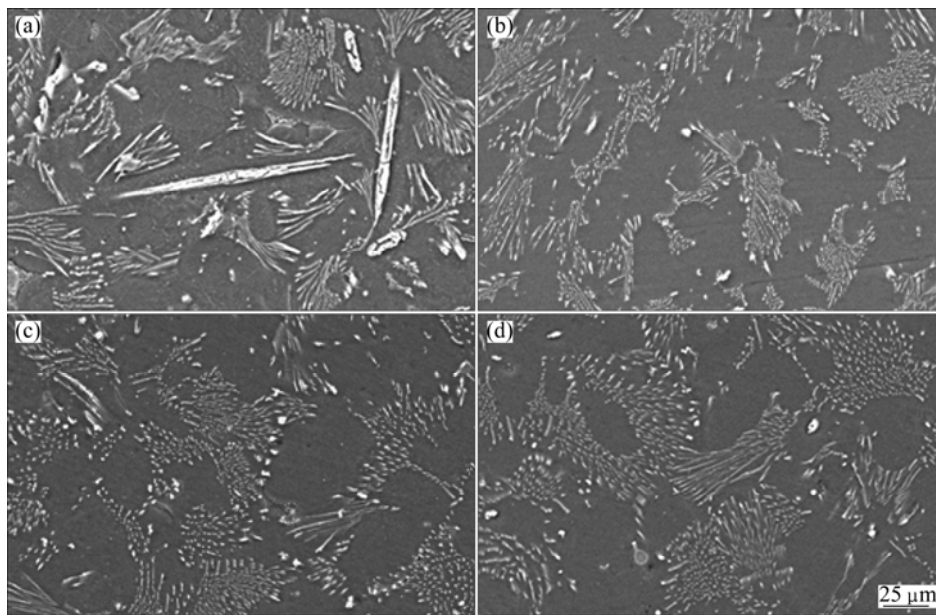


Fig. 10 SEM images of as-cast alloys after creep test at 150 °C and 70 MPa for 60 h: (a) 1[#] alloy; (b) 2[#] alloy; (c) 3[#] alloy; (d) 4[#] alloy

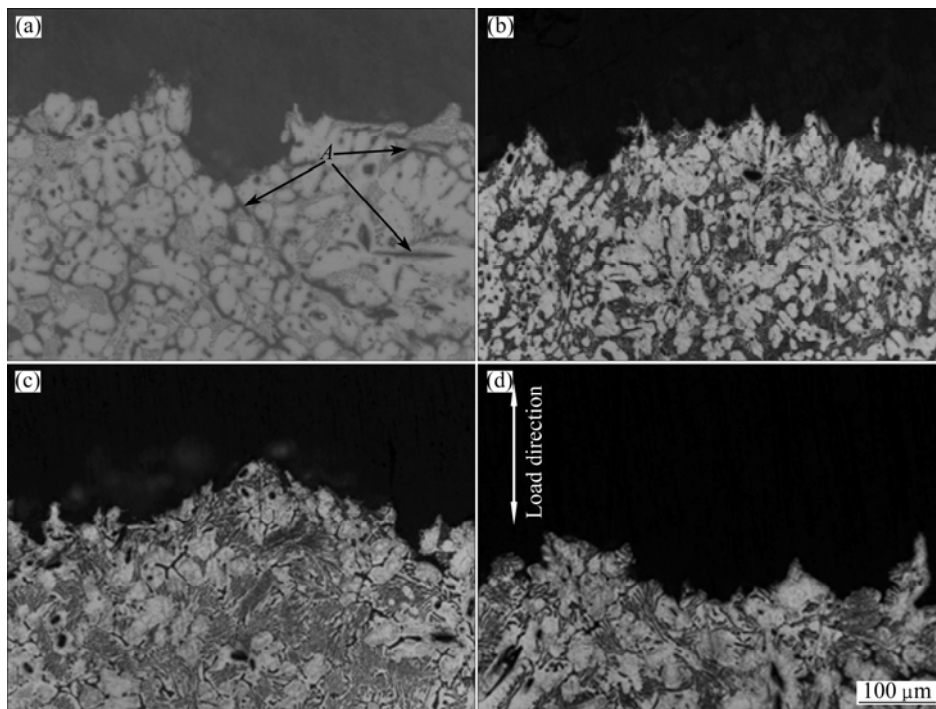


Fig. 11 Optical images of longitudinal sections for as-cast alloys obtained after creep rupture at 150 °C and 70 MPa: (a) 1[#] alloy; (b) 2[#] alloy; (c) 3[#] alloy; (d) 4[#] alloy

observed that the coarse needle-like shaped SrMgSn phases in the Mg–3Sn–2Sr ternary alloy easily act as crack initiation sites during deformation (arrow *A* in Fig. 11(a)). Therefore, another reason for the improvement in the creep properties of the Ce-, Y- and Gd-containing alloys is possibly related to the modification and refinement of the primary SrMgSn phases. Of course, the following two aspects also possibly give a beneficial effects on the creep properties of the Ce-, Y- and Gd-containing alloys: 1) the Mg₁₂Ce, YMgSn and GdMgSn phases have relatively high thermal stability [3,13–15]; 2) Ce, Y and Gd additions possibly prevent pipe diffusion by forming a solute atmosphere around the dislocations because Ce, Y and Gd elements have higher melting points than Sn and Sr elements, and then they are possibly less mobile at high temperatures than Sn and Sr. However, this needs to be further confirmed.

4 Conclusions

1) The Mg–3Sn–2Sr ternary alloy is mainly composed of α -Mg, primary and eutectic SrMgSn, and Mg₂Sn phases, thereinto the primary SrMgSn phase exhibits typical particle-, needle- and short rod-like morphologies and the eutectic SrMgSn phase exhibits typical feather-like morphology.

2) The additions of 1.0% Ce, 1.0% Y or 1.0% Gd to the Mg–3Sn–2Sr ternary alloy can suppress the formation of the primary SrMgSn phase in the alloy. At the same time, the coarse needle-like shaped primary SrMgSn phases in the Ce-, Y- and Gd-containing alloys are also modified and refined. In addition, the extra Mg₁₂Ce, YMgSn, GdMgSn and/or Mg₁₇Sr₂ phases are formed in the Ce-, Y- and Gd-containing alloys, respectively.

3) The additions of 1.0% Ce, 1.0% Y or 1.0% Gd to the Mg–3Sn–2Sr ternary alloy can simultaneously improve the tensile and creep properties of the alloy. Among the Ce-, Y- and Gd-containing alloys with similar creep properties, the tensile properties of the Ce-containing alloy are relatively higher than those of the Y- and Gd-containing alloys.

References

- [1] LUO A A, PEKGULERYUZ O. Cast magnesium alloys for elevated temperature applications [J]. *Journal of Materials Science*, 1994, 29(20): 5259–5271.
- [2] YANG M B, LI H L, DUAN C Y, ZHANG J. Effects of minor Ti addition on as-cast microstructure and mechanical properties of Mg–3Sn–2Sr (wt.%) magnesium alloy [J]. *Journal of Alloys and Compounds*, 2013, 579: 92–99.
- [3] YANG Ming-bo, QIN Cai-yuan, PAN Fu-sheng, ZHOU Tao. Comparison of effects of cerium, yttrium and gadolinium additions on as-cast microstructure and mechanical properties of Mg–3Sn–1Mn magnesium alloy [J]. *Journal of Rare Earths*, 2011, 29(6): 550–557.
- [4] NAYYERI G, MAHMUDI R. Effects of Sb additions on the microstructure and impression creep behavior of a cast Mg–5Sn alloy [J]. *Materials Science and Engineering A*, 2010, 527(3): 669–678.
- [5] NAYYERI G, MAHMUDI R. Enhanced creep properties of a cast Mg–5Sn alloy subjected to aging treatment [J]. *Materials Science and Engineering A*, 2010, 527(18–19): 4613–4618.
- [6] GU X N, XIE X H, LI N, ZHENG Y F, QIN L. In vitro and in vivo studies on a Mg–Sr binary alloy system developed as a new kind of biodegradable metal [J]. *Acta Biomaterialia*, 2012, 8(6): 2360–2374.
- [7] LI Y C, WEN C, MUSHAHARY D, SRAVANTHI R, HARISHANKAR N, PANDE G, HODGSON P. Mg–Zr–Sr alloys as biodegradable implant materials [J]. *Acta Biomaterialia*, 2012, 8(8): 3177–3188.
- [8] BORKAR H, HOSEINI M, PEKGULERYUZ M. Effect of strontium on the texture and mechanical properties of extruded Mg–1%Mn alloys [J]. *Materials Science and Engineering A*, 2012, 549: 168–175.
- [9] LIU H M, CHEN Y G, ZHAO H F, WEI S H, GAO W. Effects of strontium on microstructure and mechanical properties of as-cast Mg–5 wt.%Sn alloy [J]. *Journal of Alloys and Compounds*, 2010, 504(2): 345–350.
- [10] KIM B H, PARK K C, PARK Y H, PARK I M. Effect of Ca and Sr additions on high temperature and corrosion properties of Mg–4Al–2Sn based alloys [J]. *Materials Science and Engineering A*, 2011, 528(3): 808–814.
- [11] GORNY A, BAMBERGER M, KATSMAN A. High temperature phase stabilized microstructure in Mg–Zn–Sn alloys with Y and Sb additions [J]. *Journal of Materials Science*, 2007, 42(24): 10014–10022.
- [12] SHI Bing-qing, CHEN Rong-shi, KE Wei. Effect of element Gd on phase constituent and mechanical property of Mg–5Sn–1Ca alloy [J]. *Transactions of Nonferrous Metals Society of China*, 2010, 20(S2): s341–s345.
- [13] YANG M B, PAN F S, CHENG L, SHEN J. Effects of cerium on as-cast microstructure and mechanical properties of Mg–3Sn–2Ca magnesium alloy [J]. *Materials Science and Engineering A*, 2009, 512(1–2): 132–138.
- [14] YANG M B, PAN F S. Effects of Y addition on as-cast microstructure and mechanical properties of Mg–3Sn–2Ca (wt.%) magnesium alloy [J]. *Materials Science and Engineering A*, 2009, 525(1–2): 112–120.
- [15] YANG M B, ZHU Y, LIANG X F, PAN F S. Effects of Gd addition on as-cast microstructure and mechanical properties of Mg–3Sn–2Ca magnesium alloy [J]. *Materials Science and Engineering A*, 2011, 528(3): 1721–1726.
- [16] YANG Ming-bo, QIN Cai-yuan, PAN Fu-sheng. Effects of heat treatment on microstructure and mechanical properties of Mg–3Sn–1Mn magnesium alloy [J]. *Transactions of Nonferrous Metals Society of China*, 2011, 21(10): 2168–2174.
- [17] MANFRINETTI P, PROVINO A, GSCHNEIDNER J K A. On the RMgSn rare earth compounds [J]. *Journal of Alloys and Compounds*, 2009, 482(1–2): 81–85.
- [18] BALASUBRAMANI N, PILLAI U T S, PAI B C. Optimization of heat treatment parameters in ZA84 magnesium alloy [J]. *Journal of Alloys and Compounds*, 2008, 457(1–2): 118–123.
- [19] SPIGARELLI S, CERRI E, EVANGELISTA E, KLOC L, CADEK J. Interpretation of constant-load and constant-stress creep behavior of a magnesium alloy produced by rapid solidification [J]. *Materials Science and Engineering A*, 1998, 254(1–2): 90–98.
- [20] LUO A A. Recent magnesium alloy development for elevated temperature application [J]. *International Materials Reviews*, 2004, 49(1): 13–30.

Ce、Y 和 Gd 对 Mg–3Sn–2Sr 镁合金 铸态组织和力学性能的影响

杨明波^{1,2,3}, 侯梦丹², 张佳², 潘复生³

1. 重庆理工大学 汽车零部件制造及检测技术教育部重点实验室, 重庆 400054;
2. 重庆理工大学 材料科学与工程学院, 重庆 400054;
3. 重庆大学 国家镁合金工程材料研究中心, 重庆 400030

摘 要: 通过扫描电镜、X 射线衍射、差热分析以及抗拉和蠕变性能测试等手段, 调查和比较了 Ce、Y 和 Gd 对 Mg–3Sn–2Sr 镁合金铸态组织和力学性能的影响。结果表明: Mg–3Sn–2Sr 三元合金主要由 α -Mg、初生和共晶 SrMgSn 以及 Mg₂Sn 相组成。当添加 1.0%Ce、1.0%Y 和 1.0%Gd 到 Mg–3Sn–2Sr 合金后, 合金中分别形成了 Mg₁₂Ce、YMgSn、GdMgSn 和/或 Mg₁₇Sr₂ 相。同时, 合金中初生 SrMgSn 相的形成被抑制, 且呈针状的粗大初生 SrMgSn 相也被变质和细化。此外, 添加 1.0%Ce、1.0%Y 和 1.0%Gd 均能同时改善 Mg–3Sn–2Sr 合金的抗拉性能和蠕变性能。在含 Ce、Y 和 Gd 合金中, 含 Ce 合金的抗拉性能相对较含 Y 和含 Gd 合金的高。

关键词: Mg–Sn–Sr 镁合金; Ce; Y; Gd; SrMgSn 相

(Edited by Sai-qian YUAN)